Supplementary Information

Functional anatomy and disparity of the postcranial skeleton of African mole-rats (Bathyergidae)

Germán Montoya-Sanhueza, Nigel C Bennett, Anusuya Chinsamy, Radim Šumbera

Contents:

Supplementary Methods

Linear Measurements (Figure 2). Total bone lengths for humerus (HL), ulna (UL), femur (FL) and tibia-fibula (TL) represent the maximum distance from the proximal articular surface to the distal articular surface of each bone. In the humerus, transversal (TDH) and anteroposterior diameters (APDH) were measured below the deltoid tuberosity (~60% from proximal epiphysis). Because *H. glaber* has a different diaphyseal morphology as compared to the other species, the APDH in this taxon was measured at the major axis (i.e. the longest diameter) of the midshaft (50%), which is oriented anterolaterally. The location of the deltoid tuberosity (DLH) was measured from the humeral head to the distal origin of this structure. The humeral head diameter (HH) is the maximum distance in its major breadth (proximo-distal). Humeral (EH) and femoral (EF) epicondylar widths were measured as the maximum distance between the medial and lateral borders of the epicondyles. In the ulna, the olecranon length (OL) is the distance from the tip of the olecranon process to the center of the trochlear notch. The functional length of the ulna (FUL) is the difference between UL and OL. The transversal (TDU) and anteroposterior diameters of the ulna (APDU) correspond to the diameters at 50% from the proximal epiphysis. In the femur, the transversal diameter (TDF) was measured at the 50% of the FL from its proximal epiphysis (usually below the third trochanter). Due to the circular shape of the femoral head, its diameter (FH) was measured as the maximum distance between the medial edge to the lateral edge. In the tibio-fibula, the location of the distal tibio-fibular junction (DTFJ) was measured as the distance from the proximal articular surface to the DTFJ. The mediolateral (TDT) and anteroposterior diameters (APDT) of the tibia-fibula were measured at the DTFJ. The tibial tuberosity (UTL) was measured from the proximal articular surface to the distal point of this feature.

Supplementary Results

Humeral anatomy (Figure 3A; Supplementary Figure 1A-C)

In general, the humerus of bathyergids (except *Heterocephalus glaber*) is robust, has a large humeral head and wide epicondyles. The humeral head is hemispherical (ellipsoid) with its, longer, proximo-distal axis oriented slightly towards the lateral side of the bone. In lateral view, the humeral head is highly convex in all species, although *H. glaber* has a variable shape of the humeral head, with many specimens presenting a rather flattened humeral head and a less pronounced humeral neck. The humeral head generally grows higher as compared to the greater and lesser tubercles, although sometimes it is at similar height with the greater tubercle, which is always larger than the lesser tubercle. The intertubercular groove is well-developed in all species.

The diaphysis is relatively straight in both anterior and lateral views, and thickens towards the proximal and distal parts of the bone, although this thickening is less notorious in the distal diaphysis of *H. glaber*, which is rather narrow. All bathyergids (except *H. glaber*) present a very well-developed deltoid tuberosity in the anterolateral side of the midshaft. In *H. glaber*, this trait is highly reduced (non-projected) and sometimes indistinguishable along the diaphysis, although a small scar for the insertion of the *mm. deltoidei* is discernible in some specimens (see details in Montoya-Sanhueza et al. 2021a). In the posteromedial side, at the level of the proximal origin of the deltoid tuberosity, the teres tuberosity (*tuberositas teres major*) develops in all species, although this feature seems to be less conspicuous in *G. capensis*. The humeral torsion of the humerus is quite conspicuous, particularly discernible in posterior view.

In most bathyergids, the diaphyseal bone geometry at the midshaft is relatively circular to triangular, with the anterolateral region defining a pointy projection due to the presence of the distal origin of the deltoid tuberosity (e.g. Montoya-Sanhueza & Chinsamy, 2017). However, the diaphysis of *H. glaber* is highly compressed and lacking the deltoid tuberosity, thus resulting in a rather semi-triangular (ellipsoidal) diaphyseal cross-sectional shape (see Montoya-Sanhueza et al. 2021a). Nevertheless, the major axis (i.e. the longest diameter) of the midshaft of *H. glaber* is also oriented anterolaterally, as the deltoid tuberosity of the rest of the bathyergids.

All species showed a relatively thick development of the epicondyles, especially the medial epicondyle, which is sometimes oriented downwards in some species and individuals (e.g. *Fukomys damarensis* and *H. glaber*). The lateral epicondyle is well-developed, although associated with a reduced lateral epicondylar crest. All species have a conspicuous supratrochlear fossa, which in some individuals undergoes bone resorption, and forming the supratrochlear foramen. The topography of the distal humerus (trochlea and capitulum) of *H. glaber* is less marked and shows a more even surface in comparison to the rest of the bathyergids. As noted in previous studies (e.g. De Graaff, 1979), none of the specimens studied here showed an entepicondylar foramen in the distal humerus.

Ulnar anatomy (Figure 3A; Supplementary Figure 1D-E)

The ulna of bathyergids is elongated, generally straight, and relatively robust. The most distinctive features are the well-developed olecranon process and the relatively thick antero-posterior diameters below the trochlear notch. The morphology of the olecranon process is relatively similar among species, exhibiting a wide surface behind the anconeal process (anterior view), although this surface is wider and projects laterally in *Bathyergus suillus*. The olecranon has a nutrient foramen in its anterior surface. Both the anconeal process and the medial coronoid process are well-developed. The former rises perpendicularly to the longitudinal axis of the bone, while the latter orientates diagonally (~45°). In lateral view, below the trochlear notch, the diaphysis reaches its major anteroposterior thickness, which is thicker as compared to

the mediolateral diameter. In lateral view, below the trochlear notch, a conspicuous sulcus is formed along the midshaft, allowing a wide surface for muscle attachment. In the anterior region of the midshaft, a conspicuous scar for the interosseous ligament also develops. In anterior view, the ulna appears relatively straight in most species and specimens, although some specimens show a slight curvature, resulting in a concave medial side. This is accentuated when the tip of the proximal epiphysis tends to project internally (medially). Several specimens of *H. glaber* showed a conspicuous curved ulna.

Femoral anatomy (Figure 4A; Supplementary Figure 2A-B)

All species showed a similar femoral shape, with a robust diaphysis and well-developed epicondyles. All species showed a circular femoral head with a conspicuous femoral neck that separates the head from the trochanters, although *H. glaber* has a variable configuration of the proximal femur (see below). In all species, the greater trochanter is located at a similar height as the femoral head. The lesser trochanter is quite similar in position and size among species, and it is located lower than the femoral head, and always representing an independent structure in adulthood. However, *H. glaber* has a hemispherical femoral head and a shorter femoral neck, and several individuals showed a fused greater trochanter and femoral head. Such unusual morphology for a rodent is described in detail elsewhere (Montoya-Sanhueza et al., 2022b). The trochanteric fossa appears deeper in larger species, and shallower in smaller species. All species have a similar development of the intertrochanteric crest in terms of shape and size. All species also showed a conspicuous third trochanter, although the shape of this structure seems to vary among and within a species: it appears to cover a wider surface in solitary species, while it tends to be more localized in social species, resulting in a sharp point. This results in solitary species having a more conspicuous gluteal tuberosity (ridge), which originates at the lower part of the greater trochanter. The diaphysis is compressed in its anteroposterior axis in all species, being wider mediolaterally than anteroposteriorlly. Such compression seems to be more accentuated in *H. glaber*, resulting in having very thin anteroposterior diameters.

In lateral view, the diaphysis is straight, lacking any curvature. In anterior view, the distal region is internally (medially) orientated with respect to the longitudinal axis of the bone. The distal femur shows a wide epicondylar region and a wide patellar surface without showing the typical femoral patellar groove observed in surface-dwelling mammals (Szalay and Sargis, 2001). In general, both condyles are well-developed and project externally at a similar degree. All species showed a well-developed intercondyloid fossa.

Tibio-fibular anatomy (Figure 4A; Supplementary Figure 2C-D)

All bathyergids showed a proximal and distal fusion of the tibia and fibula, except *H. glaber* which does not fuse such bones in their distal regions. In general, the tibia is much larger and robust as compared to the fibula. In the tibia, the tibial spine is well-developed, allowing the attachment of large muscles. The non-ossified tibia and fibula of *H. glaber* are less robust, and distally united by a syndesmotic joint. A more detailed description of this feature is presented in Montoya-Sanhueza et al. (2022a).

Supplementary Tables

Supplementary Table 1

Supplementary Table 1. Results of the MANOVAs on morpho-functional indices for the forelimb and hindlimb including all species and all indices. Partial eta square (PES) values indicate the proportion of variance explaining interspecific differences (other details in Table 4 in the main text). Abbreviations: Brachial index (BI); Crural index (CI); Femoral epicondylar index (EIF); Femoral head index (FHI); Femur robustness index (FRI); Humeral epicondylar index (EIH); Humeral head index (HHI); Humerus robustness index (HRI); Index of fossorial ability (IFA); Intermembral index (IMI); Relative position of the deltoid tuberosity (RDT); Tibio-fibular junction index (TJI); Robustness of the tibia (TRI); Robustness of the tibia (TRI*); Tibial spine index (TSI); Robustness of the forearm (URI); Robustness of the forearm (URI*); Degree of freedom (Df); F-tests (F); Mean squares (MS).

Index	Df	Mean Square	F	p	Partial Eta Squared (PES)
Forelimb (all spp)					
HRI	6	0.006	51.457	<< 0.0001	0.566
HHI	6	0.008	43.678	<< 0.0001	0.525
EIH	6	0.014	44.822	<< 0.0001	0.532
IFA	6	0.013	40.206	<< 0.0001	0.504
URI	6	0.000	10.319	<< 0.0001	0.207
URI*	6	0.003	56.907	<< 0.0001	0.590
BI	6	0.145	90.806	<< 0.0001	0.697
Forelimb (all indices)					
RDT	5	0.013	23.959	<< 0.0001	0.409
HRI	5	0.001	9.744	<< 0.0001	0.220
HHI	5	0.001	5.412	<< 0.0001	0.135
EIH	5	0.005	15.016	<< 0.0001	0.303
IFA	5	0.015	49.380	<< 0.0001	0.588
URI	5	0.000	9.890	<< 0.0001	0.222
URI*	5	0.002	34.454	<< 0.0001	0.499
BI	5	0.010	5.596	<< 0.0001	0.139
Hindlimb (all spp)					
FRI	6	0.002	14.380	<< 0.0001	0.291
EIF	6	0.010	42.751	<< 0.0001	0.550
FHI	6	0.001	7.564	<< 0.0001	0.178
TSI	6	0.059	70.142	<< 0.0001	0.667
CI	6	0.081	76.605	<< 0.0001	0.686
IMI	6	0.009	16.781	<< 0.0001	0.324
Hindlimb (all indices)					
FRI	5	0.001	3.815	0.0028	0.115
EIF	5	0.008	30.219	<< 0.0001	0.507
FHI	5	0.001	11.819	<< 0.0001	0.287
TSI	5	0.020	21.848	<< 0.0001	0.426

TRI	5	0.002	29.108	<< 0.0001	0.498
TRI*	5	0.003	15.947	<< 0.0001	0.352
TJI	5	0.029	43.891	<< 0.0001	0.599
CI	5	0.089	90.036	<< 0.0001	0.754
IMI	5	0.010	16.221	<< 0.0001	0.356

Supplementary Table 2

Supplementary Table 2. Correlation coefficients of the $PCA_{F1\text{-}F2}$ and $PCA_{H1\text{-}H1}$ for the morpho-functional indices of the forelimb and hindlimb, respectively, including all species and all indices. See abbreviations of indices in Supplementary Table 2.

Forelimb	**PC 1**	**PC 2**	**PC 3**	**PC 4**	**PC 5**	**PC 6**
All species						
BI	0.722	-0.013	-0.037	0.008	-0.022	-0.002
HRI	0.617	0.035	0.228	0.105	0.044	0.047
HHI	0.532	0.074	-0.239	0.029	0.239	0.004
EIH	0.574	0.064	0.457	-0.065	0.061	-0.011
IFA	0.030	0.822	-0.038	-0.021	-0.024	0.002
URI*	-0.521	0.180	0.286	0.465	-0.033	-0.021
URI	-0.084	-0.280	0.279	-0.140	-0.213	0.083
All indices						
RDT	0.291	0.677	-0.005	0.024	0.003	
HRI	0.224	0.097	0.402	-0.104	0.009	
HHI	-0.037	-0.065	-0.315	-0.015	0.227	
EIH	0.120	-0.111	0.604	-0.118	0.050	
IFA	-0.761	0.186	0.141	0.234	0.006	
URI	0.295	-0.163	0.262	-0.040	-0.237	
URI*	-0.173	0.666	0.265	-0.208	0.038	
BI	0.313	-0.089	0.052	0.213	0.008	
Hindlimb	**PC 1**	**PC 2**	**PC 3**	**PC 4**	**PC 5**	**PC 6**
All species						
FRI	-0.115	0.478	0.048	-0.239	0.050	0.061
EIF	0.345	0.875	0.020	0.050	-0.076	0.024
FHI	-0.026	0.346	0.117	0.323	0.144	0.062
TSI	-0.569	0.392	-0.210	-0.002	0.010	-0.007
CI	0.851	0.191	-0.068	-0.007	0.012	-0.006
IMI	-0.270	0.567	0.498	-0.011	0.016	-0.017
All indices						
FRI	0.075	0.373	-0.074	0.105	0.118	
EIF	0.607	0.555	0.319	-0.013	-0.087	
FHI	0.050	0.448	0.122	-0.311	-0.195	
TSI	-0.546	0.223	0.134	-0.190	0.021	
CI	0.859	-0.015	0.117	-0.014	0.017	
IMI	-0.142	0.749	0.049	0.150	0.000	
TJI	-0.501	-0.182	0.489	0.067	0.015	
TRI*	-0.010	0.644	-0.135	-0.081	0.131	
TRI	-0.624	-0.018	-0.242	0.368	0.000	

Supplementary Table 3

Supplementary Table 3. Jackknifed cross-validations of group assignments obtained from the discriminant analysis (LDA) including all species (LDA_1; n = 216) and all indices (LDA_2; n = 152). For LDA_1, a total of 93.06% correctly classified individuals were obtained. The misclassified individuals are indicated with an asterisk (*) and pertained to the solitary chisel-tooth digger and social chisel-tooth digger groups, accumulating 6.94% (15 individuals). For LDA_2, a total of 97.37% correctly classified individuals were obtained. The misclassified individuals are indicated with an asterisk (*) and pertained mostly to the solitary chisel-tooth digger, accumulating only 0.97% (4 individuals). Groups: solitary scratch-digger (1); solitary chisel-tooth digger (2); and social chisel-tooth digger (3).

Jackknifed (All species)				
Groups	1	2	3	Total
1	39	0	0	39
2	0	47	4	51
3	0	11	115	126
Total	39	58	119	216
% correctly classified				93.06
Jackknifed (All indices)				
Groups	1	2	3	Total
1	39	0	0	39
2	0	48	3	51
3	0	1	61	62
Total	39	49	64	152
% correctly classified				97.37

Supplementary Table 4

Supplementary Table 4. Descriptive statistics and Mann-Whitney U-test for assessment of sex differences in body mass (BM). Significance ($p < 0.05$) is indicated with an asterisk (*).

Species	n	Mean ± s.d. Females			n	Mean ± s.d. Males			Mann-Whitney U-test	Mann-Whitney p
B. suillus	23	798.870	±	282.637	16	1141.813	±	370.434	91	0.008*
He. argenteocinereus	16	173.163	±	51.313	12	177.453	±	55.965	93	0.908
G. capensis	32	180.273	±	62.627	15	152.902	±	60.071	164.5	0.087
F. mechowii	8	157.075	±	93.280	5	270.120	±	117.353	10	0.164
F. damarensis	9	86.549	±	33.590	10	140.000	±	47.896	13.5	0.011*
C. hottentotus	13	58.550	±	13.115	19	74.632	±	23.554	73	0.055
H. glaber	28	30.690	±	9.895	24	31.700	±	11.322	335	0.993

Supplementary Table 5

Supplementary Table 5. Two-way PERMANOVA analysis of the effect of species and sex in morpho-functional indices. All species included, except *Heterocephalus glaber* (see text). Significance ($p < 0.05$) is indicated with an asterisk (*). Degree of freedom (Df); F-tests (F); Mean squares (MS); Sum of squares (SS).

	Df	SS	MS	F	p
Species	5	1.031	0.206	21.497	0.0001*
Sex	1	0.005	0.005	0.563	0.584
Interaction	5	-0.303	-0.061	-6.327	0.408
Residual	178	1.707	0.010		
Total	189	2.440			

Supplementary Figures

Supplementary Figure 1

Supplementary Figure 1. Details of the humeral and ulnar anatomy of *Georychus capensis*. A) Anterior, B) posterior, and C) lateral views of left humerus of a large male specimen. D) Anterior, and E) lateral views of ulna of same specimen. Small bones silhouettes show the real relative size of bones among species. The humeri are aligned to the distal origin of the deltoid tuberosity (except in *Heterocephalus glaber*), while the ulnae are aligned to the centre of the trochlear notch.

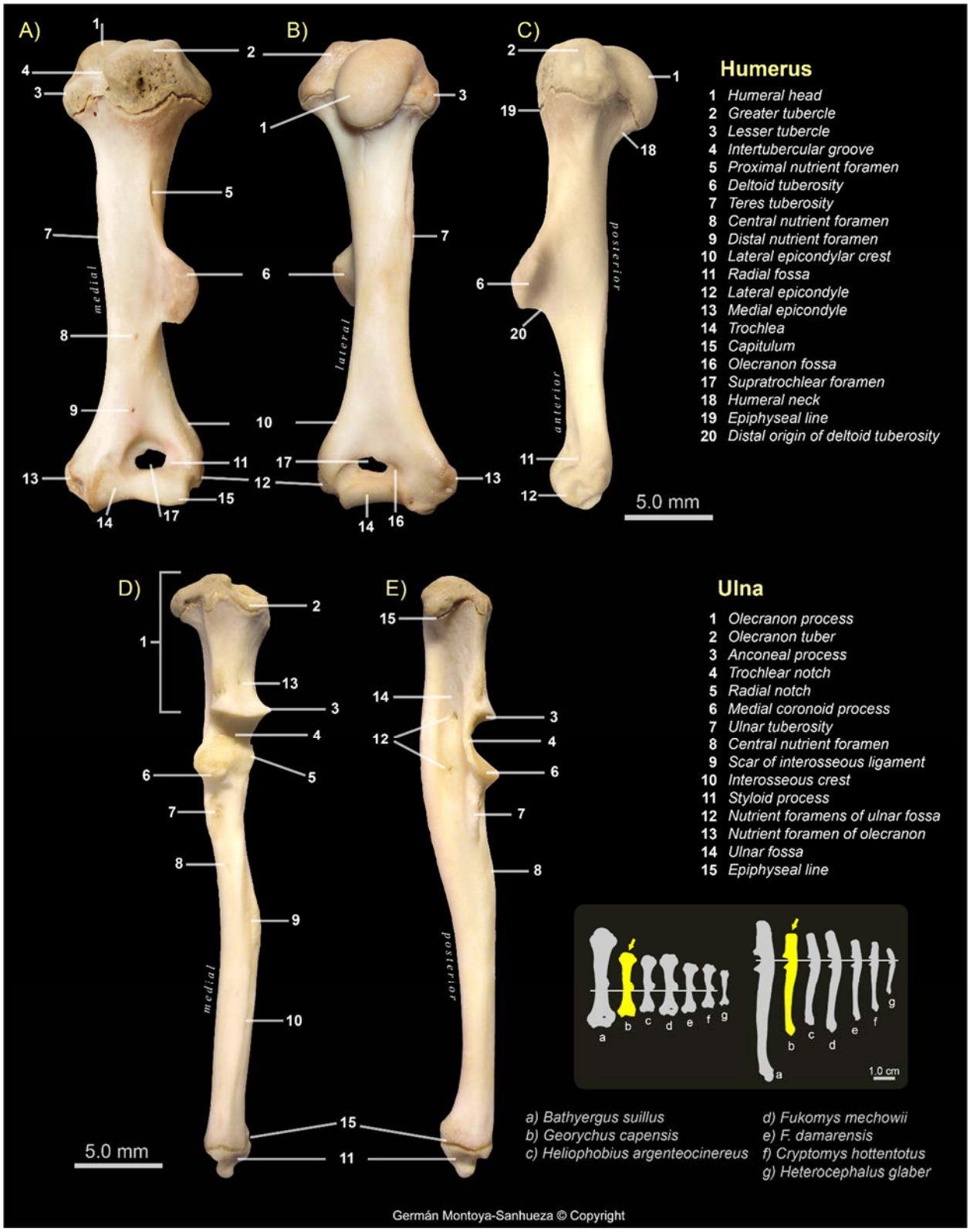
A)
B)
C)
D)
E)
medial
lateral
posterior
anterior
5.0 mm
Humerus
1 Humeral head
2 Greater tubercle
3 Lesser tubercle
4 Intertubercular groove
5 Proximal nutrient foramen
6 Deltoid tuberosity
7 Teres tuberosity
8 Central nutrient foramen
9 Distal nutrient foramen
10 Lateral epicondylar crest
11 Radial fossa
12 Lateral epicondyle
13 Medial epicondyle
14 Trochlea
15 Capitulum
16 Olecranon fossa
17 Supratrochlear foramen
18 Humeral neck
19 Epiphyseal line
20 Distal origin of deltoid tuberosity
Ulna
1 Olecranon process
2 Olecranon tuber
3 Anconeal process
4 Trochlear notch
5 Radial notch
6 Medial coronoid process
7 Ulnar tuberosity
8 Central nutrient foramen
9 Scar of interosseous ligament
10 Interosseous crest
11 Styloid process
12 Nutrient foramens of ulnar fossa
13 Nutrient foramen of olecranon
14 Ulnar fossa
15 Epiphyseal line
1.0 cm
a) Bathyergus suillus
b) Georychus capensis
c) Heliophobius argenteocinereus
d) Fukomys mechowii
e) F. damarensis
f) Cryptomys hottentotus
g) Heterocephalus glaber
Germán Montoya-Sanhueza © Copyright

Supplementary Figure 2

Supplementary Figure 2. Details of the femoral and tibio-fibular anatomy of *Georychus capensis*. A) Anterior, and B) posterior views of left femur of same specimen as Supplementary Figure 1. D) Anterior and E) medial views of left tibia-fibula of same specimen. Small bones silhouettes show the real relative size of bones among species. The femora are aligned to the distal origin of the third trochanter, while the tibia-fibulae are aligned to the distal tibio-fibular junction (except in *Heterocephalus glaber*).

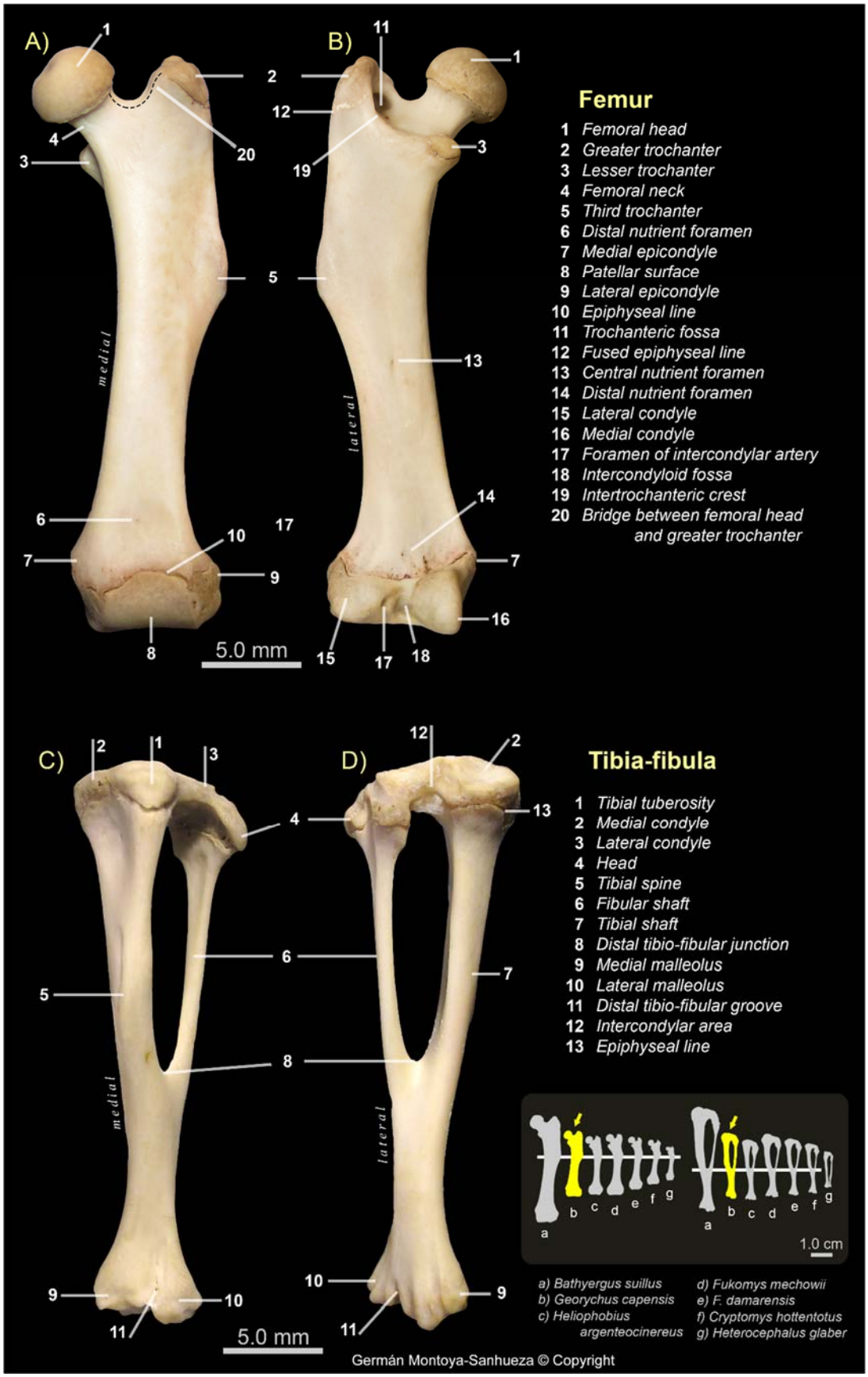
A)
B)
C)
D)
medial
lateral
5.0 mm
Femur
1 Femoral head
2 Greater trochanter
3 Lesser trochanter
4 Femoral neck
5 Third trochanter
6 Distal nutrient foramen
7 Medial epicondyle
8 Patellar surface
9 Lateral epicondyle
10 Epiphyseal line
11 Trochanteric fossa
12 Fused epiphyseal line
13 Central nutrient foramen
14 Distal nutrient foramen
15 Lateral condyle
16 Medial condyle
17 Foramen of intercondylar artery
18 Intercondyloid fossa
19 Intertrochanteric crest
20 Bridge between femoral head and greater trochanter
Tibia-fibula
1 Tibial tuberosity
2 Medial condyle
3 Lateral condyle
4 Head
5 Tibial spine
6 Fibular shaft
7 Tibial shaft
8 Distal tibio-fibular junction
9 Medial malleolus
10 Lateral malleolus
11 Distal tibio-fibular groove
12 Intercondylar area
13 Epiphyseal line
1.0 cm
a) Bathyergus suillus
b) Georychus capensis
c) Heliophobius argenteocinereus
d) Fukomys mechowii
e) F. damarensis
f) Cryptomys hottentotus
g) Heterocephalus glaber
Germán Montoya-Sanhueza © Copyright

Supplementary Video

Direct link to YouTube: https://youtu.be/YpvqOSp1KUU

The video recordings show captive individuals of *Heterocephalus glaber* performing digging behavior with fore- and hindlimbs in captive colonies at University of Cape Town. The colonies were kept in glass containers lacking any substrate to dig. The first video (00:08-00:45) shows an old mature individual using a combination of chisel-tooth digging and scratch-digging. The second video (00:46-01:19) shows an individual performing backwards hindlimb digging, typically used to push the soil out of the burrow. Despite this colony has been maintained without soil or any other substrates, the colony members perform intense and repetitive digging behavior, indicating its strong innate nature. This colony was established in the early 1980's by Emeritus Associate Professor Jenny Jarvis, and its animals have ended up in different laboratories in the USA, UK, Germany, France, Japan, South Korea, China and Israel (De Blocq, 2016). Videos were recorded in January 2014, in the Department of Biological Sciences at the University of Cape Town. Copyright © Germán Montoya-Sanhueza. Video Editing: Floriane Blanc Marquis. Emeritus Professor Jenny Jarvis is acknowledged for allowing the recording of the specimens. Sources: De Blocq, A (2016) 'Bon voyage' to UCT's naked mole rats. https://andrewdeblog.weebly.com/home/bon-voyage-to-ucts-naked-mole-rats

Supplementary References

- De Graaff, G. (1979). Molerats (Bathyergidae, Rodentia) in South African National Parks: notes on the Taxonomic "isolation" and Hystricomorph Affinities of the family. Koedoe, 22(1): a653.

- Montoya-Sanhueza, G and A. Chinsamy. (2017). Long bone histology of the subterranean rodent *Bathyergus suillus* (Bathyergidae): ontogenetic pattern of cortical bone thickening. J Anat, 230(2): 203-233.

- Montoya-Sanhueza G, Bennett NC, Oosthuizen MK, Dengler-Crish CM, Chinsamy A. (2021). Long bone histomorphogenesis of the naked mole-rat: histodiversity and intraspecific variation. J Anat 238(6): 1259–1283.

- Montoya-Sanhueza, G, Šumbera, R, Bennett, NC and A Chinsamy. (2022). Developmental Plasticity in the Ossification of the Proximal Femur of *Heterocephalus glaber* (Bathyergidae, Rodentia). J Mammal Evol https://doi.org/10.1007/s10914-022-09602-y

- Szalay FS, and Sargis E J. (2001). Model-based analysis of postcranial osteology of marsupials from the Palaeocene of Itaboraí (Brazil) and the phylogenetics and biogeography of Metatheria. Geodiversitas 23(2): 139-302.